Probing the Molecular Dynamics of the ABC Multidrug Transporter LmrA by Deuterium Solid-State Nuclear Magnetic Resonance†

Alena Siarheyeva,‡ Jakob J. Lopez,‡ Ines Lehner,‡ Ute A. Hellmich,‡ Hendrik W. van Veen,§ and Clemens Glaubitz*,‡

Institute for Biophysical Chemistry and Centre for Biomolecular Magnetic Resonance, J. W. Goethe Universität, Frankfurt am Main, Germany, and Department of Pharmacology, University of Cambridge, Cambridge, U.K.

Received October 10, 2006; Revised Manuscript Received January 5, 2007

ABSTRACT: The molecular dynamics of the 64 kDa ABC multidrug efflux pump LmrA from *Lactococcus lactis* within lipid membranes has been investigated by deuterium solid-state NMR. Deuteriomethyl-labeled alanine has been used to probe global protein backbone dynamics. A comparison of static deuterium NMR spectra of full-length LmrA in the resting state and its isolated transmembrane domain revealed a high mobility for the nucleotide binding domains. Their motional freedom is restricted upon ATP binding as seen for LmrA in complex with AMP-PNP, a nonhydrolyzable ATP analogue. LmrA returns to full motional flexibility in the posthydrolysis, vanadate-trapped state. These experiments provide insight into the molecular dynamics of a full-length ABC transporter during the catalytic cycle. Data are discussed in the context of known biochemical data and structural models of ABC transporters.

ATP-binding cassette (ABC)[1] transporters are integral membrane proteins that couple ATP binding and hydrolysis with transport of various molecules across cellular membranes. Found in both prokaryotes and eukaryotes, a subgroup of these transporters is involved in the efflux of hydrophobic drugs and lipids, causing antimicrobial and chemotherapeutic multidrug resistance (MDR). Because of their importance, a wealth of experimental information is available.

ABC transporters have four core domains. Two transmembrane domains (TMDs) consist of multiple membrane-spanning α-helices, which form a pathway for substrates across the lipid bilayer. Two nucleotide binding domains (NBDs) contain the ATP binding sites and couple conformational changes induced by ATP binding and hydrolysis and release of ADP and P_i to the transport process. These four domains have been found encoded as separate polypeptides or fused into multidomain proteins (*1*).

Due to structure and sequence similarities in NBDs of different transporters, it is generally accepted that they bind and hydrolyze ATP in a similar fashion and therefore possibly use a common mechanism to power the translocation of substrate across the membrane. Our understanding of the mechanism of ABC transporters is based on low-resolution structures of P-glycoprotein (PGP) obtained at several stages of the transport cycle and is supported by a number of biochemical assays. Analysis of two-dimensional crystals of PGP by cryo-electron microscopy revealed major conformational changes within the TMDs upon ATP binding. As a consequence, drug binding affinity is reduced and a central pore opens across the membrane. These conformational changes can, potentially, facilitate movement of hydrophobic compounds from the lipid bilayer to the aqueous pore of the transporters (*2*, *3*). Crystal structures of a number of isolated NBDs supplemented with a plethora of biochemical investigations have been obtained in recent years (*4*−*10*). A dimer with a head-to-tail orientation is found in the crystal structures of ABC domain MJ1267 of *Methanococcus janaschii* and RLI ABC ATPase RNase-L inhibitor of *Pyrococcus furiosus* (*7*, *11*). Biochemical studies and molecular dynamics simulations have suggested that ATP binding initiates NBD dimerization but hydrolysis destabilizes the NBD dimer followed by its dissociation (*12*−*14*).

So far, four full-length ABC transporter crystal structures of bacterial origin were obtained (*15*−*18*). These structures provide snapshots of several defined conformations and support the view that conformational rearrangements within NBDs and TMDs are connected to each other. These rearrangements might be associated with an altered molecular dynamics, which requires further studies.

Here, we report a deuterium NMR study which provides insight into the dynamics of the ABC multidrug efflux pump LmrA of *Lactococcus lactis*. LmrA is the first discovered and so far the best characterized bacterial ABC MDR transporter. It is a structural homologue of PGP in bacteria.

† This research was supported by SFB 628 'Functional Membrane Proteomics'. A.S. acknowledges a scholarship from the International Max-Planck-Research School Frankfurt.

* To whom correspondence should be addressed: Institut für Biophysikalische Chemie, J. W. Goethe Universität, Max von Laue Str. 9, 60438 Frankfurt am Main, Germany. Telephone: +49-69-79829927. Fax: +49-69-79829929. E-mail: glaubitz@em.uni-frankfurt.de.

‡ J. W. Goethe University.

§ University of Cambridge.

[1] Abbreviations: ABC, ATP-binding cassette; AMP-PNP, adenylylimidodiphosphate; ATR-FTIR, attenuated total reflection Fourier transform infrared; EPR, electron paramagnetic resonance; ICD, intracellular domain; ISOV, inside-out vesicle; LmrA-MD, NBD deficient LmrA mutant; $LmrA_{prot}$, transmembrane domain of LmrA obtained by limited proteolysis; MDR, multidrug resistance; NBD, nucleotide binding domain; NMR, nuclear magnetic resonance; PGP, P-glycoprotein; TMD, transmembrane domain.

10.1021/bi062109a CCC: $37.00
Published on Web 02/16/2007

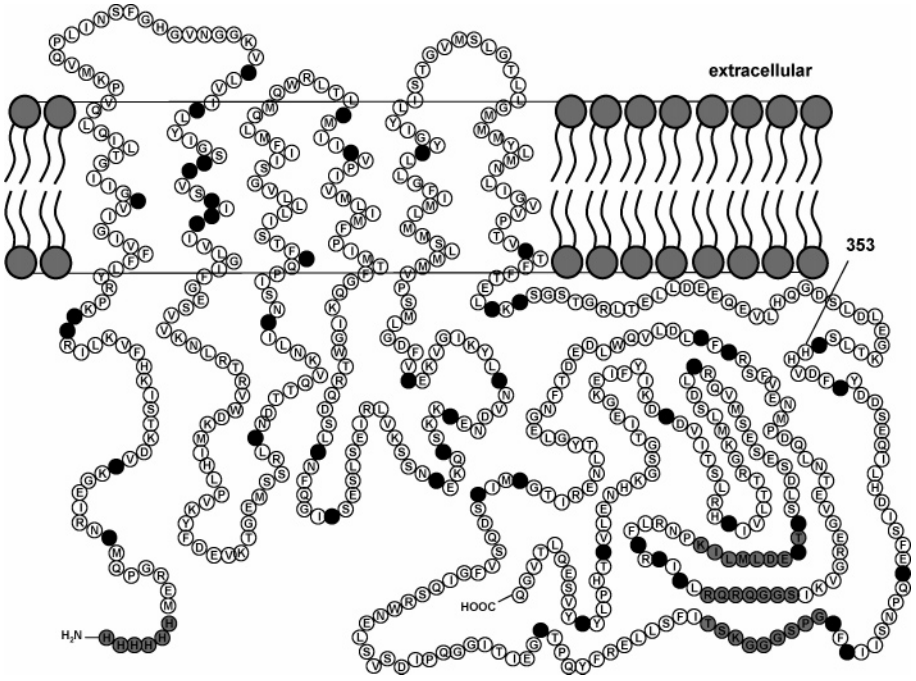

FIGURE 1: Schematic membrane topology of the *L. lactis* multidrug transporter LmrA monomer reveals a distribution of 12 alanines in the transmembrane domain (TMD), 17 in loops and the intercellular domain (ICD), and 19 in the nucleotide binding domain (NBD) (black). In LmrA-MD, NBDs are cut off at residue His-353. Walker-A, Walker-B, C-loop, and His tag are labeled in gray.

LmrA can functionally substitute PGP in lung fibroblast cells and shares its substrate specificity (*19*). The minimal functional unit in the LmrA transporter is the homodimer. Each of both 590-residue monomers contains six membrane-spanning regions (putative α-helices) in the amino-terminal hydrophobic domain, followed by a large hydrophilic domain with an ATP binding site (*20*).

Deuterium solid-state NMR is a convenient method for probing macromolecular dynamics. In contrast to liquids, the orientation-dependent NMR parameters of protein motions are not averaged out by the rapid overall tumbling of the protein (*21*, *22*). Deuterium spin−lattice relaxation times T_{1Z} and T_{1Q} are most sensitive to motions with correlation times on the order of the inverse of the Larmor frequency (e.g., 92 MHz at 14 T). The spectral line shapes report on motions on the time scale of the inverse of the quadrupole coupling constant (e^2qQ/h) (=167 kHz for a C−D group in a rigid lattice). In the intermediate exchange region, when motion rates are equal to the quadrupole coupling constant, T_2 becomes comparable to the time delay in the quadrupole echo experiment which results in a loss of signal. This might cause problems with relating spectral intensities to the number of deuterons contributing to them. Line shape analysis is simplified by the very often axially symmetric deuterium quadrupole coupling tensor (asymmetry parameter $\eta \approx 0$). The dynamic processes accessible with deuterium NMR stretch over correlation times between 10^{-10} and 10^{-4} s which cover rotational diffusion of membrane proteins, wobbling about the bilayer normal, internal motions, and side chain reorientations (*23*). In the past, the dynamics of proteins or bound ligands has been extensively studied using ^{2}H solid-state NMR (*23*−*28*).

To probe protein dynamics of LmrA, we have labeled the protein with L-[β-$^2H_3$]alanine (Figure 1). Alanine side chains were chosen because of their direct attachment to the α-carbon which allows monitoring of the protein backbone dynamics. Thus, any motions influencing the line shape, other than threefold methyl reorientation about the $C_\alpha-C_\beta$ bond axis, must arise from the protein backbone (*25*). ^{2}H NMR spectra of LmrA in its resting state were obtained. Data are compared to those of LmrA-MD, a truncated LmrA protein lacking the NBD and to those of LmrA in prehydrolysis (complexed with AMP-PNP) and posthydrolysis states (trapped upon the addition of vandate and ATP).

EXPERIMENTAL PROCEDURES

Microorganisms and Media. L. lactis strain NZ9000 was used as a host for expression vector pNH LmrA and LmrA-MD. LmrA-MD is an N-terminally His_6-tagged LmrA truncated in the linker region at His-353 that connects the transmembrane with the nucleotide binding domains (*29*). *L. lactis* strain NZ9700 was used for nisin production. Cells were cultured overnight at 30 °C in M17 medium (BD, Sparks, MD) supplemented with 0.5% (w/v) glucose and 5 μg/mL chloramphenicol. They were used to inoculate large-scale cultures in labeling medium which were grown at 30 °C without shaking. Protein expression was carried out as described previously (*30*).

Labeling. LmrA and LmrA-MD were labeled with L-[β-$^2H_3$]alanine by growing *L. lactis* on a chemically defined medium (*30*) which contained only half the required amount of alanine (0.15 g/L). Protein expression was initiated at an OD_{660} of 0.4. At that point, additional 0.15 g/L L-[β-$^2H_3$]-alanine was added, and bacteria were induced with 1% nisin after 15 min. The bacterial growth was followed by measuring the OD_{660} every 40 min on a UV-550 Jasco spectrophotometer. Cells were harvested when the OD_{660} reached 0.9. All amino acids were obtained from Sigma-Aldrich.

Protein Purification and Reconstitution. Preparation of inside-out vesicles (ISOVs) was carried out as described previously (*31*). For purification of histidine-tagged LmrA,

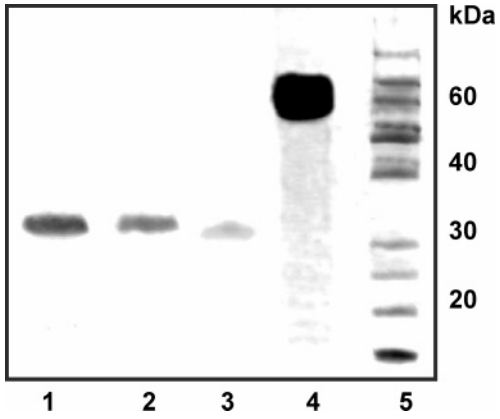

FIGURE 2: SDS−PAGE of LmrA-MD (36 kDa) (1), the membrane-bound component of $LmrA_{prot}$ after proteolysis (35 kDa) (2), LmrA-NBD left in the supernatant after proteolysis (3), and full-length LmrA (64 kDa) (4). Molecular mass standards are given in column 5.

L. lactis ISOVs were solubilized on ice with the solubilization buffer [100 mM Tris, 50 mM NaCl, 10% (v/v) glycerol, and 3% (w/v) DDM (pH 8.0)] for 1 h. The unsolubilized fraction was removed by ultracentrifugation (55 000 rpm for 40 min). The supernatant was incubated with Ni-NTA agarose for 1 h on ice. Ni-NTA agarose was preliminarily pre-equilibrated with buffer A [100 mM Tris, 50 mM NaCl, 10% (v/v) glycerol, 0.05% (w/v) DDM, and 10 mM imidazole (pH 8.0)]. After the incubation, the resin was loaded on a column (Pharmacia) attached to an Äkta Prime FPLC system (Pharmacia). Non-histidine-tagged proteins were washed from the column with buffers A and B [100 mM Tris, 50 mM NaCl, 10% (v/v) glycerol, 0.05% (w/v) DDM, and 10 mM imidazole (pH 8.0 and 7.0, respectively)]. When no further protein was detected in the flow (OD monitored at 280 nm), LmrA was eluted with buffer B supplemented with 250 mM imidazole. The purification was carried out at 4 °C and was verified using SDS−PAGE (Figure 2). In addition, sample homogeneity was checked by analytical gel filtration. Both SDS−PAGE and gel filtration confirmed high protein purity (95%) without any aggregation. *n*-Dodecyl β-D-maltoside (DDM) was from Glycon Biochemicals GmbH (Luckenwalde, Germany); Ni^{2+} nitriloacetic acid (Ni-NTA) resin was from Qiagen Inc., and all other chemicals were from Sigma-Aldrich.

Reconstitution was essentially carried out as described previously using *Escherichia coli* total lipid extract (Avanti Polar Lipids, Alabaster, AL) at a starting molar ratio of 250 lipids per protein. Detergent was removed with SM2 bio-beads (Bio-Rad Laboratories). To minimize deuterium natural abundance, the proteoliposomes containing LmrA were further resuspended in buffer [100 mM Tris and 50 mM KCl (pH 7)] made from deuterium-depleted water (Sigma-Aldrich). Samples were pelleted by centrifugation for 40 min at 50 000 rpm. The procedure was repeated twice for each preparation.

AMP-PNP and ADP·Vanadate Complexes of LmrA. To create LmrA in a prehydrolysis state, proteoliposomes were resuspended in a total volume of 5 mL of buffer containing 20 mM AMP-PNP, a nonhydrolyzable ATP analogue, and 5 mM $MgCl_2$. The sample was incubated for 30 min on a rocking table at room temperature. To create a posthydrolysis state, proteoliposomes were incubated in 5 mL of buffer containing 2 mM vanadate, followed by addition of 20 mM ATP. The samples were pelleted by centrifugation at 55 000 rpm for 40 min. The procedure was repeated twice for each preparation. After the second washing step, proteoliposomes were immediately transferred into a 4 mm MAS rotor.

LmrA-MD. Purification and reconstitution of LmrA-MD were carried out as they were for LmrA. LmrA-MD (LmrA truncated at His-353) was detected as a 36 kDa protein by SDS−PAGE (Figure 2).

Proteolysis of LmrA ($LmrA_{prot}$). As an alternative to LmrA-MD, NBDs were removed from LmrA by proteolysis (*32*). Proteoliposomes of LmrA (3 mg/mL) were incubated with proteinase K (4 mg/mL) at room temperature on a rocking table for 30 min. The proteolytic digestion was stopped by addition of phenylmethanesulfonyl fluoride (Serva) to a final concentration of 1 mM. Proteoliposomes containing LmrA-MD and $LmrA_{prot}$ were further resuspended in buffer made of deuterium-depleted water and pelleted by centrifugation for 40 min at 55 000 rpm. The procedure was repeated twice for each preparation. The sample was analyzed by SDS−PAGE (Figure 2). After being washed and pelleted, samples were transferred into 4 mm MAS rotors.

^{2}H NMR Measurements. All ^{2}H NMR experiments were performed on a Bruker Avance 600 spectrometer equipped with a 4 mm MAS DVT probe. The measurements were conducted at a ^{2}H Larmor frequency of 92.123 MHz. For all static measurements, a $90_x°-\tau-90_y°-\tau-$echo experiment was used (*33*). The acquisition time was 8.123 ms, the 90° pulse 4 μs, the recycle delay time 0.4 s, and the echo delay 50 μs. The spectral width for ^{2}H was set to 300 kHz. Spectra were zero-filled to 4096 points, and up to 2500 Hz exponential line broadening was applied during processing. Approximately 100K acquisitions were accumulated. Experiments were repeated for three independent membrane preparations, of which each contained approximately 4 mg of LmrA. All spectra were processed and analyzed using Topspin (Bruker, Karlsruhe, Germany).

The temperature was regulated using a Bruker BCU temperature control unit. Variable-temperature experiments always started at the lowest temperatures. Samples were rapidly frozen in liquid nitrogen to prevent formation of ice crystals.

Spectra were deconvoluted into two spectral components by fitting the sum of two ^{2}H spectra with respect to their individual quadrupole coupling constants, intensities, and line widths to the experimental data (Figure 3).

Deuterium T_1 relaxation times were measured using the inversion recovery method with a quadrupole echo for observation ($180°-$delay$-90_x°-\tau-90_y°-\tau-$echo). To analyze partially relaxed ^{2}H spectra with different spectral components, a linear combination, with the linear coefficients as fitting parameters, was used to approximate the measured signal. A plot of the respective linear coefficients over the mixing time resulted in exponential inversion recovery curves for each component and was used to obtain T_1.

^{31}P NMR Experiments. To probe membrane integrity and to test for the occurrence of unilamellar vesicles, static ^{31}P NMR spectra of the samples used for ^{2}H NMR were recorded at 7 °C. In addition, empty liposomes were prepared as described above, including detergent destabilization and detergent removal. The sample was pelleted by centrifugation

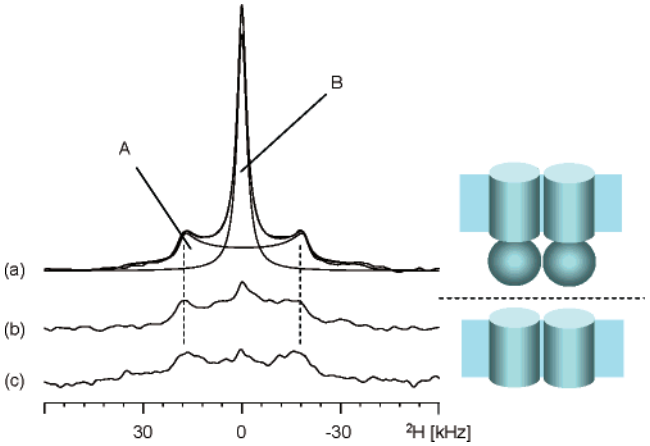

FIGURE 3: ^{2}H spectrum of Ala-d_3-LmrA which can be decomposed into two distinct spectral components, A and B (a). Component A is a typical Pake pattern with 37.5 kHz splitting (50 kHz quadrupole coupling constant), while component B can be simulated by an isotropic line. A signal arises from 48 alanines (144 deuterons) in loops, nucleotide binding domains, and transmembrane domains. This isotropic component is not observed in Ala-d_3-LmrA-MD, a NBD deficient mutant (b), or after enzymatic removal of the NBDs from Ala-d_3-LmrA$_{prot}$ (c). All three proteins were reconstituted into *E. coli* lipids (250:1 molar ratio). Spectra were recorded at 7 °C. The amount of protein was between 2 and 4 mg.

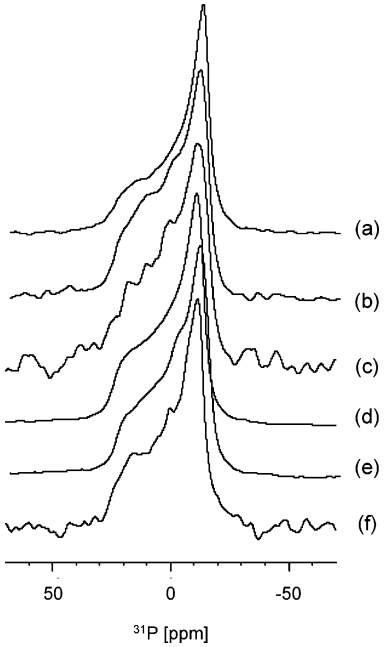

FIGURE 4: Static ^{31}P NMR spectra of *E. coli* liposomes without protein (a), with LmrA-MD (b), with LmrA$_{Prot}$ (c), with full-length LmrA in complex with ATP·vanadate (d), with AMP-PNP (e), and in its resting state (f). The lipid:protein molar ratio was 250:1 in all cases. Spectra were acquired at 7 °C. For all samples, typical line shapes corresponding to an axially symmetric ^{31}P CSA tensor were obtained. There were no signs of unilamellar vesicles which would cause isotropic lines due to fast tumbling.

for 30 min at 50 000 rpm and transferred into a 4 mm MAS rotor.

The ^{31}P measurements were performed on a Bruker Avance 400 spectrometer equipped with a 4 mm MAS DVT probe. The measurements were performed at 161.923 MHz. The ^{31}P spectra were acquired using a Hahn echo pulse sequence (*34*), with an echo delay of 15 μs and a ^{31}P excitation pulse with a length of 3 μs. Continuous wave ^{1}H decoupling was applied during the acquisition. A line broadening of 500 Hz was applied to all spectra. The number of scans collected for each measurement was 4K.

RESULTS

^{2}H NMR on LmrA in Its Resting State with and without Nucleotide Binding Domains. A deuterium quadrupole echo spectrum of Ala-d_3-LmrA at 7 °C is shown in Figure 3a. The temperature was not increased above 7 °C to ensure protein stability and activity over the time course of the experiment. The spectrum can be described by two components. Component A is a Pake pattern with 37.5 kHz splitting, while component B can be described by an isotropic line. The difference between the best fit of components A and B and the experimental spectrum is shown in Figure 5a. The ratio of the peak areas of component A to B is 1.1. The line width of B measured after Fourier transformation without exponential line broadening is 125 Hz. Using an inversion recovery experiment, we have also determined the T_1 relaxation times (averaged over all orientations) for both components to be 20 ± 2 (A) and 28 ± 2 ms (B) (see the Supporting Information). At lower temperatures, component B gradually disappears. Below −23 °C, a typical Pake pattern with a 39 kHz splitting and the total loss of component B are observed and T_1 is 14 ± 1 ms. At −23 °C the total spectral intensity is 20% higher compared to that at 7 °C (Figure 5a).

A likely explanation for the appearance of this isotropic component is a collapse of the quadrupole coupling due to motional averaging in parts of LmrA. The reorientation of deuterons over a wide angular range has to take place within a time period which is much smaller than the inverse of the frequency of the rigid quadrupolar coupling, i.e., less than 10^{-5} s (*25*). Such a situation could most likely arise within flexible nucleotide binding domains and/or in the loop regions of LmrA (Figure 1).

To identify domains of LmrA with potentially high molecular mobility, we have carried out further ^{2}H NMR experiments on samples in which the NBD has been removed (Figure 3b,c). We have prepared Ala-d_3-LmrA-MD, a LmrA mutant which does not contain the NBD (*29*). In addition, the NBD was enzymatically cleaved off from full-length Ala-d_3-LmrA.

Although the expression of LmrA-MD was weaker than that of LmrA, sufficient amounts of labeled protein could be prepared. As in previous observations (*29*), LmrA-MD was detected via SDS−PAGE at 36 kDa (Figure 2). As for full-length LmrA, the spectrum of LmrA-MD was recorded at 7 °C. It is as broad as component A in Figure 3a and features a strongly reduced central component (Figure 3b).

To isolate the membrane-embedded domain of Ala-d_3-LmrA, proteoliposomes were treated with proteinase K (*32*). Although proteinase K nonspecifically cleaves at the carboxyl side of several aliphatic, aromatic, or hydrophobic residues, van Veen, Ruysschaert, and co-workers (*32*) could show that this protein contains all residues from loops and helices belonging to the predicted membrane domain of LmrA. This is confirmed by SDS−PAGE (Figure 2). Only one single band at 35 kDa is observed. The ^{2}H NMR line shape obtained from Ala-d_3-LmrA$_{prot}$ is similar to that of Ala-d_3-LmrA-MD, while the central component is slightly smaller (Figure 3c).

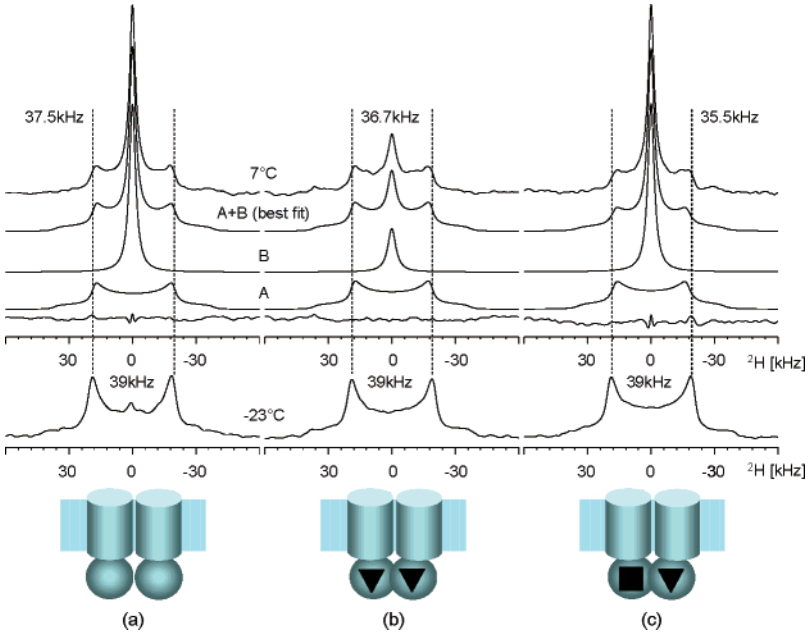

FIGURE 5: ^{2}H NMR spectra of Ala-d_3-LmrA in its resting state without added nucleotide (a), in complex with AMP-PNP for trapping a prehydrolysis state (b), and in the ADP·vanadate-trapped state which corresponds to a posthydrolysis situation (c). A Pake pattern with a 39 kHz splitting typical for a deuteriomethyl group is observed in all three cases at −23 °C. Increasing the temperature 7 °C causes an overall loss in spectral intensity between 20% in panels a and c and 40% in panel b. Furthermore, spectra can be deconvoluted into two distinct spectral components. The quadrupole splitting of component A is reduced from 39 to 35−37 kHz. The narrow component B is significantly reduced in the prehydrolysis state.

The quadrupolar splittings of Ala-d_3-LmrA$_{prot}$ and Ala-d_3-LmrA-MD are identical to that of component A of Ala-d_3-LmrA within the error of the measurements.

Verification of Membrane Integrity by ^{31}P NMR. One of the possible origins for the occurrence of an isotropic, central component could be fast molecular tumbling of protein associated with nonbilayer lipid complexes or small unilamellar vesicles. To exclude this possibility, ^{31}P static NMR was used to monitor potential changes in the phase behavior of phospholipid bilayers upon interaction with LmrA. A comparison of static ^{31}P spectra of LmrA and LmrA-MD proteoliposomes with *E. coli* lipid vesicles prepared in the same way (including detergent destabilization and detergent removal) shows similar, axially symmetric powder spectra in all cases (Figure 4). These line shapes are typical for fluid lipid bilayers. *E. coli* total lipid extract as used here for reconstitution has been shown to have a rather broad phase transition between 4 and 20 °C (*35*). Small unilamellar vesicles would cause an isotropic ^{31}P resonance which has not been observed. Additionally, freeze-fracture micrographs of samples prepared using the same procedures clearly demonstrate a reproducibly homogeneous incorporation of LmrA into liposomes (*30*).

^{2}H NMR on Ala-d_3-LmrA in Pre- and Posthydrolysis States. In Figure 5, pre- and posthydrolysis states are compared with LmrA in its resting state. Below −23 °C, a typical Pake pattern with a 39 kHz splitting, similar to values obtained for a deuteriomethyl group in solid alanine (*36*), is observed in all three cases. The dominating molecular motion at this temperature is the very fast threefold reorientation of the methyl group. Increasing the temperature reveals a second spectral component with differing intensities.

The spectral features of resting-state LmrA have been described above. Figure 5a shows the ^{2}H spectrum obtained at 7 °C, the result of fitting two components to the line shape, the difference between the best fit experimental spectrum and a ^{2}H spectrum obtained at −23 °C.

Corresponding data for LmrA in a pre- and posthydrolysis state are shown in panels b and c of Figure 5, respectively. To investigate dynamic properties of LmrA under ATP binding, the nonhydrolyzable ATP analogue AMP-PNP was used instead of ATP. This analogue has been used extensively to trap several ABC transporters, including PGP and LmrA in a prehydrolysis state (*2*, *37*). To trap LmrA in a posthydrolysis state, ATP was added together with vanadate. Vanadate traps ADP at one of the two nucleotide-binding sites by mimicking the transition state of the γ-phosphate of ATP during hydrolysis. In addition, vanadate trapping at one site inhibits ATP hydrolysis at the second site (*10*, *31*, *38*). For efficient trapping of LmrA in both, all ATP binding sites have to be accessible to ATP and should not be buried in the lumen of the vesicles. Although we have not carried out additional experiments to assess the ATP binding site accessibility, strong evidence that ATP binding domains are facing the outside in our reconstituted samples exists (*29*). ATPase activity of LmrA in reconstituted form is similar to that of inside-out vesicles (*30*). In addition, proteinase K cleavage results in a complete removal of NBDs due to their uniform orientation within the vesicles.

^{2}H NMR data of LmrA in complex with AMP-PNP are shown in Figure 5b. At 7 °C, the central component is strongly reduced compared to that depicted in Figure 5a. The ratio of component A to B is 3.7. The quadrupole splitting of component A is reduced to 36.7 kHz. The line width of component B obtained from data processed without line broadening is 1400 Hz. At −23 °C, a typical Pake pattern is obtained which has 40% more integral spectral intensity than the spectrum recorded at 7 °C.

Interestingly, the magnitude of the central component increases again in the posthydrolysis state trapped by addition

of vanadate and ATP (Figure 5c). In this case, the intensity ratio of both spectral components (A:B) is 0.9, i.e., almost identical to that of the LmrA resting state. Component B has a true line width of 140 Hz. The total integral spectral intensity is reduced by 20% when the temperature is increased from −23 to 7 °C.

DISCUSSION

Structural and dynamic information about membrane proteins in their membrane-embedded form is difficult to obtain. While X-ray crystallography has advanced in the field of ABC transporters and three-dimensional structures of MsbA, BtuCD, and Sav1866 have been published (*15*−*17*), there is still a lack of information about molecular dynamics. Here, we have provided qualitative insight by low-resolution ^{2}H NMR into Ala-d_3-LmrA in three different states. The main finding is that a large number of deuterons are located in molecular segments which undergo fast reorientations. Most importantly, the nucleotide binding domains but not the loop regions have been identified to cause the detected isotropic spectral component.

Ala-d_3-LmrA in the Resting State. At low temperatures, the spectrum of Ala-d_3-LmrA in the resting state assumes the form of a typical Pake pattern with a quadrupole coupling close to CD_3 groups in solids (39 kHz). The observed splitting does change slightly with an increase in temperature (37.5 kHz) which is most likely caused by libration or hopping of the alanine side chains and by tumbling and rotational diffusion of the whole protein within the membrane. In addition, the overall line shape is characterized by the occurrence of a dominant isotropic component (Figures 3a and 5a). The experiments with Ala-d_3-LmrA-MD and Ala-d_3-$LmrA_{prot}$ provide strong evidence that this isotropic component originates from the LmrA NBDs as this peak is removed from the spectrum with removal of the NBDs from the sample (Figure 3b,c). This observation indicates that the NBDs tumble much faster than 10^{-5} s while the transmembrane domains remain slow on this time scale since the broad spectral component does not change significantly with temperature. The observed loss of 20% of the total signal intensity with a temperate increase from −23 to 7 °C also indicates that parts of the protein undergo motions on the intermediate time scale (microseconds). Attempts to investigate these motions in detail by varying the quadrupole echo delay time were not successful due to the limited signal-to-noise ratio of the samples used here. However, an educated guess allows an explanation of the observed intensities. We have 19 alanines in the NBDs contributing to component B and 12 alanines in the TMDs and 17 alanines within the ICD which could contribute to component A. This would give an A:B ratio of ≈3:2, but analysis of Figure 3a returns a ratio of 1:1. The difference could indeed be caused by intermediate motions. It is reasonable to assume that in particular the broad component is affected by this intensity loss. If we take this into account, we find that (A + 20%):B ≈ (TMD + ICD):NBD ≈ 3:2.

The high mobility of deuterons contributing to component B (NBD) in Figure 3a should also be reflected in their T_1 relaxation time which has been determined to be 28 ± 2 ms. In comparison, component A (TMD) exhibits a relaxation time of 20 ± 2 ms. The difference between both is smaller than one might expect. A comparison with model compounds indicates a trend with increasing motional correlation times. The T_1 values at 7 °C of solid, zwitterionic Ala-d_3, Ala-d_3 in solution (100 mM), and D_2O were determined to be 4 ± 1 ms (averaged over all orientations), 160 ± 1 ms, and 232 ± 1 ms, respectively (data not shown; see the Supporting Information). This increase in T_1 with decreasing correlation times agrees with a relaxation time analysis of deuteriomethyl-labeled amino acids by Oldfield and co-workers (*39*). A further, more quantitative interpretation of our data would require a temperature-dependent analysis of T_1 of both components, including T_1 anisotropy. But even if these data would become available, their analysis would be rather complicated due to spectral overlap of many different deuterons from different parts of LmrA.

High molecular mobility within LmrA has been noted before by ATR-FTIR spectroscopy and ^{1}H−^{2}H exchange (*32*). The authors concluded there is motional flexibility within the transmembrane domain of LmrA. This observation is consistent with our data. Although the quadrupole splitting of the spectra arising from the transmembrane domains was only slightly reduced (Figure 3), the observed loss of signal intensity indicates motions in the intermediate time scale regime. In addition, we have observed a high flexibility of the NBDs. This dynamic regime is most likely caused by rapid movements of the whole domains combined with internal fluctuations. The latter is supported by a number of experimental hints. The purification of isolated NBDs is problematic in the absence of nucleotide, pointing out that nucleotide free NBDs are intrinsically unstable (*14*). High *B*-factors, describing a decrease in X-ray scattering intensity arising from thermal motions or crystal disorder, have been observed for the NBD in the nucleotide-free apo form of MsbA. They are likely to originate from high NBD mobility. A *B*-factor analysis of isolated MJ1267 NBD crystal structures in the presence and absence of ADP-Mg supports this observation (*40*). In addition, molecular dynamics simulations of the separated NBD HisP have shown that certain domains exhibit motion on a time scale of nanoseconds (*41*).

The ^{2}H spectra exhibited by both truncated versions of LmrA show similar line shapes (Figure 3b,c), and SDS−PAGE shows a similar molecular mass (Figure 2). The isotropic component in the $LmrA_{prot}$ spectrum is slightly smaller than that in the LmrA-MD spectrum which could be caused by a shorter C-terminus. Indeed, the $LmrA_{prot}$ estimated molecular mass is ∼35 kDa (*32*), while the LmrA-MD estimated molacular mass is 36 kDa (*29*). The fact that LmrA-MD does not show a larger central component and that proteolysis cleaves off just the NBDs supports the hypothesis that the intracellular loop regions are highly structured and might be relatively immobile. Indeed, the X-ray crystal structures of Sav1866 from *Staphylococcus aureus* and low-resolution cryo-microscopy structures of PGP show that ABC transporters possess a third, intracellular domain (ICD) (*16*, *42*). This domain consists mainly of α-helices. It is believed to be in contact with NBDs and to be directly involved in the communication between the NBDs and TMDs (*16*). For LmrA, no three-dimensional crystal structure of the protein is available, but a homology model could provide insight into possible loop conformations (*43*). Thus, the extracellular LmrA loops are short and therefore

probably relatively immobile. Their single alanine is unlikely to contribute significantly to the central component in the ^{2}H LmrA resting-state spectrum. The intracellular loops connecting TM helices 2 and 3, helices 4 and 5, and TM helix 6 and NBD together form predominantly α-helical ICD (*43*), which serve as an extension of TMD and might share dynamic characteristics with it. The data presented here allow a clear interpretation, but a number of potential errors have to be considered.

Naturally occurring deuterium in water could contribute to the observed isotropic central component. However, the natural abundance of deuterium is just 0.015%. The active volume of the 4 mm MAS rotors used here is ca. 50 μL which would result in 900 nmol of deuterons when completely filled with water which compares to 9000 nmol in the case of 4 mg of LmrA as used here. As the protein/lipid sample takes up most of the rotor volume, much less water is actually present which has also been deuterium depleted, reducing the amount of deuterons in water to 0.00005%. However, as deuterons arising from LmrA are spread over a large frequency range, even small traces of HDO could contribute to an isotropic line shape. Residual HDO trapped inside the vesicles could give rise to a small isotropic water peak. This contribution has been investigated by ^{2}H MAS NMR (not shown), because it is not seen in the static spectra. A small contribution of residual HDO was found to be roughly the same for all samples studied here. Therefore, samples can be compared, and the contribution of HDO to the central component in the static ^{2}H NMR spectra is assumed to be constant in all spectra and provides only a minor contribution to the spectral intensity. Interestingly, MAS did not yield an improvement in spectral intensity when compared to static spectra. This could be caused by molecular motions of LmrA in an intermediate dynamic regime in the order of the MAS sample rotation rate (microseconds). In this situation, MAS NMR loses its advantage of high resolution and sensitivity.

Partially degraded LmrA protein, disengaged from the proteoliposomes, or cross-labeled soluble proteins which remain associated after the purification procedure could be another source for isotropic spectra to appear. Keniry et al. (*44*) have observed isotropic ^{2}H line shapes from purple membrane samples which disappeared after introduction of a density gradient purification step (*45*). Here, the possibility of contamination can be excluded as SDS−PAGE analysis (Figure 2) and gel filtration did show that the protein is isolated to high purity.

The formation of unilamellar vesicles which could tumble fast enough to produce isotropic spectra has been excluded by ^{31}P NMR (Figure 4).

In view of all the data, we can conclude that this central isotopic component originates from the alanine residues located in NBDs. The NBDs are not embedded in the lipid matrix which allows a high degree of freedom, leading to very different motional characteristics compared to those of the TMDs. The central isotropic component has a dramatically reduced quadrupolar coupling. Such a reduction can be caused by contributions from fast tumbling of the NBDs, overall rotation of LmrA, and fast internal molecular fluctuations. A similar ^{2}H spectrum containing two components has been obtained for deuterated fd coat protein. The rigid part of the spectrum was assigned to immobile alanine residues, whereas the dynamic part arises from alanine residues in protein segments experiencing fast motions (*25*).

Ala-d_3-LmrA in the Pre- and Posthydrolysis States. To investigate the effect of binding of AMP-PNP on LmrA dynamics, deuterium NMR spectra of L-[β-$^2H_3$]alanine-labeled LmrA in complex with AMP-PMP and ADP·vanadate were recorded (Figure 5b,c). The binding of AMP-PNP to LmrA leads to clear changes in the LmrA spectrum (Figure 5b). The ratio of integral spectral intensities of component A to B increases from 1.1 to 3.7. The central component has an increased true line width of 1400 Hz. One possible interpretation would be that fewer deuterons take part in fast molecular reorientations. Parts of the remaining isotropic signal could also arise from resting-state LmrA in equilibrium with AMP-PNP-bound LmrA. However, this interpretation has to be taken with care. It would be also theoretically possible that parts of the proteins undergo changes in the intermediate time scale regime causing line broadening and loss of signal which would also influence the A:B ratio. These effects would be mainly expected within the transmembrane domain and could be influenced, for example, by an altered rotational diffusion of LmrA. This interpretation cannot be excluded but seems less likely as AMP-PNP binding directly affects the NBDs and not the TMDs.

As the central component has been shown to arise mainly from deuterons located in the NBDs, our observations suggest a restricted mobility of these NBDs in complex with AMP-PNP but more motional flexibility in the vanadate-trapped state.

Interestingly, the 7 °C spectrum of Ala-d_3-LmrA trapped with ADP·vanadate features an almost identical central resonance as seen in the resting state. These data show that resting-state and AMP-PNP-bound conformations are motionally different, while the ADP·vanadate-trapped LmrA is more similar to the resting state.

In the past, conformational nonequivalence between resting states and AMP-PNP-bound states has been reported for two-dimensional crystals of PGP and three-dimensional crystals of MsbA, by cross-linking studies, by cysteine accessibility tests, and by mass spectroscopy on LmrA and PGP (*2*, *37*, *38*, *46*, *47*). It has been reported that two-dimensional crystals formed more readily in the presence of AMP-PNP, suggesting that this compound induces a favorable conformation for crystal formation possibly due to lower protein flexibility (*2*). The most recent three-dimensional structure of the ABC transporter Sav1866 has been obtained with the conformational equilibrium shifted to the ATP-bound state (*16*). In this structure, both NBDs are in close contact which would allow less motional flexibility, supporting the interpretation of our data in Figure 5b.

Results in the Context of Biochemical Data. The observed NBD mobility can be caused by fast tumbling of the whole NBD together with fast internal fluctuations. NBD dimerization upon AMP-PNP binding would cause a restriction in the molecular tumbling rate. Indeed, a large number of biochemical studies and molecular dynamics simulations demonstrate that ATP binding initiates NBD dimerization (*12*, *14*).

Recent studies on the MalK ABC domain have shown that ATP promotes dimerization whereas ADP does not (*48*). The dimerization process seems to have two components. First,

binding of ATP to Walker A/B and Q loop motifs reorients the NBD1 domains. Second, recognition of the ATP γ-phosphates by the signature motifs from the opposing NBD2 induces a clamplike motion in the NBD to form a tight NBD−ATP−NBD sandwich (*7*).

ATP hydrolysis occurs when a water molecule attacks the γ-phosphate. As a result, the P−O bond, which connects the γ-phosphate, is broken. In the next step, the tight dimerization of NBDs is disrupted, as buildup of negative charge on the leaving γ-phosphate causes a disengagement of the interacting ATP binding cassettes (*49*). This results in a conformation which can be modeled by formation of the ADP·vanadate-trapped state. This model is in line with the recent *Salmonella typhimurium* MsbA crystal structure obtained in the presence of ADP and vanadate, which shows that the NBD dimer is essentially disintegrated (*50*).

NBD dimerization upon ATP binding and subsequent disintegration of the dimer after hydrolysis must lead to substantial changes in the molecular flexibility of the NBDs in a full-length transporter. These changes can explain the ^{2}H NMR data presented here. In addition, internal fluctuations are altered as well, as seen by a solution NMR study of an isolated NBD of *M. janaschii* MJ1267. ADP binding was found to alter the flexibility of key ABC motifs. It is further suggested that the transition between rigidity and flexibility in NBDs is crucial for mechanochemical energy transduction in ABC transporters and that the restriction of the protein motions can be important for allosteric communications (*51*). The hypothesis that the flexibility of NBDs is altered between different nucleotide-bound states is also supported by large *B*-factor changes in MJ1267 crystal structures in the presence and absence of ADP-Mg (*40*).

For the coupling of ATP hydrolysis to the transport cycle, a power stroke has been suggested which requires dimerization of NBDs. Whether ATP binding or ATP hydrolysis is needed to trigger such an event is still unclear and currently under debate (*32*, *52*).

SUMMARY AND CONCLUSIONS

The work presented here is the first attempt to obtain insight into the overall dynamics of full-length ABC transporter LmrA. Although site-resolved data could not be obtained by ^{2}H NMR, it could be shown that the NBDs are more mobile than transmembrane and intracellular domains in the LmrA resting state. Upon ATP binding, NBD mobility becomes restricted but is released again after hydrolysis. These observations are consistent with models of NBD dimerization based on data obtained for other ABC transporters. Future studies will utilize ^{13}C and ^{15}N labeling approaches in combination with MAS NMR to gain site-resolved insight into LmrA dynamics during the transport and catalytic cycle.

ACKNOWLEDGMENT

We thank Dr. James Mason for his initial help in establishing isotope labeling procedures.

SUPPORTING INFORMATION AVAILABLE

Spectra of LmrA and its transmembrane domain (Figure S1), spectra of LmrA in its resting and pre- and posthydrolysis states (Figure S2), partially relaxed inversion recovery spectra of resting-state LmrA (Figure S3), fitting of inversion recovery data of components A and B of LmrA (Figure S4), and fitting of inversion recovery data of model compounds (Figure S5). This material is available free of charge via the Internet at http://pubs.acs.org.

REFERENCES

1. Higgins, C. F., Hiles, I. D., Salmond, G. P. C., Gill, D. R., Downie, J. A., Evans, I. J., Holland, I. B., Gray, L., Buckel, S. D., Bell, A. W., and Hermodson, M. A. (1986) A family of related ATP-binding subunits coupled to many distinct biological processes in bacteria, *Nature 323*, 448−4450.
2. Rosenberg, M. F., Kamis, A. B., Callaghan, R., Higgins, C. F., and Ford, R. C. (2003) Three-dimensional structures of the mammalian multidrug resistance P-glycoprotein demonstrate major conformational changes in the transmembrane domains upon nucleotide binding, *J. Biol. Chem. 278*, 8294−8299.
3. Rosenberg, M. F., Velarde, G., Ford, R. C., Martin, C., Berridge, G., Kerr, I. D., Callaghan, R., Schmidlin, A., Wooding, C., Linton, K. J., and Higgins, C. F. (2001) Repacking of the transmembrane domains of P-glycoprotein during the transport ATPase cycle, *EMBO J. 20*, 5615−5625.
4. Karpowich, N., Martsinkevich, O., Millen, L., Yuan, Y. R., Dai, P. L., MacVey, K., Thomas, P. J., and Hunt, J. F. (2001) Crystal structure of the MJ1267 ATP binding cassette reveal an induced-fit effect at the ATPase active site of an ABC transporter, *Structure 9*, 571−586.
5. Yuan, Y. R., Blecker, S., Martsinkevich, O., Millen, L., Thomas, P. J., and Hunt, J. F. (2001) The crystal structure of the MJ0796 ATP-binding cassette. Implications for the structural consequences of ATP hydrolysis in the active site of an ABC transporter, *J. Biol. Chem. 276*, 32313−32321.
6. Gaudet, R., and Wiley, D. C. (2001) Structure of the ABC ATPase domain of human TAP1, the transporter associated with antigen processing, *EMBO J. 20*, 4964−4972.
7. Karcher, A., Büttner, K., Märtens, B., Jansen, R.-P., and Hopfner, K. P. (2005) X-ray structure of PLI, an essential twin cassette ABC ATPase involved in ribosome biogenesis and HIV capsid assembly, *Structure 13*, 649−659.
8. Lewis, H. A., Buchanan, S. G., Burley, S. K., Conners, K., Dickey, M., Dorwart, M., Fowler, R., Gao, X., Guggino, W. B., Hendrickson, W. A., Hunt, J. F., Kearins, M. C., Lorimer, D., Maloney, P. C., Post, K. W., Rajashankar, K. R., Rutter, M. E., Sauder, J. M., Shriver, S., Thibodeau, P. H., Thomas, P. J., Zhang, M., Zhao, X., and Emtage, S. (2004) Structure of nucleotide-binding domain 1 of the cystic fibrosis transmembrane conductance regulator, *EMBO J. 23*, 282−293.
9. Schmitt, L., Benabdelhak, H., Blight, M. A., Holland, I. B., and Stubbs, M. T. (2003) Crystal structure of the nucleotide-binding domain of the ABC-transporter haemolysin B: Identification of a variable region within ABC helical domain, *J. Mol. Biol. 330*, 333−342.
10. Fetsch, E. E., and Davidson, A. L. (2002) Vanadate-catalyzed photocleavage of the signature motif of an ATP-binding cassette (ABC) transporter, *Proc. Natl. Acad. Sci. U.S.A. 99*, 9685−9690.
11. Smith, P. C., Karpowich, N., Millen, L., Moody, J. E., Rosen, J., Thomas, P. J., and Hunt, J. F. (2002) ATP binding to the motor domain from an ABC transporter drives formation of a nucleotide sandwich dimer, *Mol. Cell 10*, 139−149.
12. Oloo, E. O., and Tieleman, D. P. (2004) Conformational transitions induced by the binding of MgATP to the vitamin B-12 ATP-binding cassette (ABC) transporter BtuCD, *J. Biol. Chem. 279*, 45013−45019.
13. van der Does, C., and Tampé, R. (2004) How do ABC transporter drive transport? *Biol. Chem. 385*, 927−933.
14. Zaitseva, J., Jenewein, S., Wiedenmann, A., Benabdelhak, H., Holland, I. B., and Schmitt, L. (2005) Functional characterization and ATP-induced dimerization of the isolated ABC-domain of the haemolysin B transporter, *Biochemistry 44*, 9680−9690.
15. Locher, K. P., Lee, A. T., and Rees, D. C. (2002) The *E. coli* BtuCD structure: A framework for ABC transporter architecture and mechanism, *Science 296*, 1091−1098.

16. Dawson, R. J. P., and Locher, K. P. (2006) Structure of a bacterial multidrug ABC transporter, *Nature 443*, 180−185.
17. Chang, G., and Roth, C. B. (2001) Structure of MsbA from *E. coli*: A homolog of the multidrug resistance ATP binding cassette (ABC) transporters, *Science 293*, 1793−1800.
18. Chang, G. (2003) Structure of MsbA from *Vibrio cholera*: A multidrug resistance ABC transporter homolog in a closed conformation, *J. Mol. Biol. 330*, 419−430.
19. van Veen, H. W., Callaghan, R., Soceneantu, L., Sardini, A., Konings, W. N., and Higgins, C. F. (1998) A bacterial antibiotic-resistance gene that complements the human multidrug-resistance P-glycoprotein gene, *Nature 391*, 291−295.
20. van Veen, H. W., Venema, K., Bolhuis, H., Oussenko, I., Kok, J., Poolman, B., Driessen, A. J. M., and Konings, W. N. (1996) Multidrug resistance mediated by a bacterial homolog of the human multidrug transporter MDR1, *Proc. Natl. Acad. Sci. U.S.A. 93*, 10668−10672.
21. Torchia, D. A., and Szabo, A. (1982) Spin-Lattice Relaxation in Solids, *J. Magn. Reson. 49*, 107−121.
22. Torchia, D. A. (1984) Solid-state NMR studies of protein internal dynamics, *Annu. Rev. Biophys. Bioeng. 13*, 125−144.
23. Prosser, R. S., and Davis, J. H. (1994) Dynamics of an integral membrane peptide: A deuterium NMR relaxation study of gramicidin, *Biophys. J. 66*, 1429−1440.
24. Jelinski, L. W., Sullivan, C. E., and Torchia, D. A. (1980) ^{2}H NMR study of molecular motion in collagen fibrils, *Nature 284*, 531−534.
25. Leo, G. C., Colnago, L. A., Valentine, K. G., and Opella, S. J. (1987) Dynamics of fd coat protein in lipid bilayers, *Biochemistry 26*, 854−862.
26. Copie, V., Mcdermott, A. E., Beshah, K., Williams, J. C., Spijkerassink, M., Gebhard, R., Lugtenburg, J., Herzfeld, J., and Griffin, R. G. (1994) Deuterium solid-state nuclear-magnetic-resonance studies of methyl-group dynamics in bacteriorhodopsin and retinal model compounds: Evidence for a 6-*s*-*trans* chromophore in the protein, *Biochemistry 33*, 3280−3286.
27. Williamson, P. T. F., Watts, J. A., Addona, G. H., Miller, K. W., and Watts, A. (2001) Dynamics and orientation of $N^+(CD_3)_3$-bromoacetylcholine bound to its binding site on the nicotinic acetylcholine receptor, *Proc. Natl. Acad. Sci. U.S.A. 98*, 2346−2351.
28. Rozovsky, S., and McDermott, A. E. (2001) The time scale of the catalytic loop motion in triosephosphate isomerase, *J. Mol. Biol. 310*, 259−270.
29. Venter, H., Shilling, R. A., Velamakanni, S., Balakrishnan, L., and van Veen, H. W. (2003) An ABC transporter with a secondary-active multidrug translocator domain, *Nature 426*, 866−870.
30. Mason, A. J., Siarheyeva, A., Haase, W., Lorch, M., van Veen, H., and Glaubitz, C. (2004) Amino acid type selective isotope labelling of the multidrug ABC transporter LmrA for solid-state NMR studies, *FEBS Lett. 568*, 117−121.
31. van Veen, H. W., Margolles, A., Muller, M., Higgins, C. F., and Konings, W. N. (2000) The homodimeric ATP-binding cassette transporter LmrA mediates multidrug transport by an alternating two-site (two-cylinder engine) mechanism, *EMBO J. 19*, 2503−2514.
32. Grimard, V., Vigano, C., Margolles, A., Wattiez, R., van Veen, H. W., Konings, W. N., Ruysschaert, J. M., and Goormaghtigh, E. (2001) Structure and dynamics of the membrane-embedded domain of LmrA investigated by coupling polarized ATR-FTIR spectroscopy and H-1/H-2 exchange, *Biochemistry 40*, 11876−11886.
33. Davis, J. H., Jeffrey, K. R., Bloom, M., Valic, M. I., and Higgs, T. R. (1976) Quadrupolar echo deuteron magnetic resonance spectroscopy in ordered hydrocarbon chains, *Chem. Phys. Lett. 42*, 390−394.
34. Rance, M., and Byrd, R. A. (1984) Obtaining high-fidelity spin-1/2 powder spectra in anisotropic media: Phase-cycled Hahn echo spectroscopy, *J. Magn. Reson. 52*, 221−240.
35. Killian, J. A., Fabrie, C. H. J. P., Baart, W., Morein, S., and Dekruijff, B. (1992) Effects of temperature-variation and phenethyl alcohol addition on acyl chain order and lipid organization in *Escherichia coli* derived membrane systems: A H-2-NMR and P-31-NMR study, *Biochim. Biophys. Acta 1105*, 253−262.
36. Beshah, K., Olejniczak, E. T., and Griffin, R. G. (1987) Deuterium NMR study of methyl group dynamics in L-alanine, *J. Chem. Phys. 89*, 4730−4736.
37. Ecker, G. F., Pleban, K., Kopp, S., Csaszar, E., Poelarends, G. J., Putman, M., Kaiser, D., Konings, W. N., and Chiba, P. (2004) A three-dimensional model for the substrate binding domain of the multidrug ATP binding cassette transporter LmrA, *Mol. Pharmacol. 66*, 1169−1179.
38. Loo, T. W., and Clarke, D. M. (2002) Vanadate trapping of nucleotide at the ATP-binding sites of human multidrug resistance P-glycoprotein exposes different residues to the drug-binding site, *Proc. Natl. Acad. Sci. U.S.A. 99*, 3511−3516.
39. Keniry, M. A., Kintanar, A., Smith, R. L., Gutowsky, H. S., and Oldfield, E. (1984) Nuclear magnetic-resonance studies of amino-acids and proteins: Deuterium nuclear magnetic-resonance relaxation of deuteriomethyl-labeled amino-acids in crystals and in *Halobacterium halobium* and *Escherichia coli* cell membranes, *Biochemistry 23*, 288−298.
40. Karpowich, N., Martsinkevich, O., Millen, L., Yuan, Y. R., Dai, P. L., MacVey, K., Thomas, P. J., and Hunt, J. F. (2001) Crystal structure of the MJ1267 ATP binding cassette reveal an induced-fit effect at the ATPase active site of an ABC transporter, *Structure 9*, 571−586.
41. Campbell, J. D., Deol, S. S., Ashcroft, F. M., Kerr, I. D., and Sansom, M. S. P. (2004) Nucleotide-dependent conformational changes in HisP: Molecular dynamics simulations of an ABC transporter nucleotide-binding domain, *Biophys. J. 87*, 3703−3715.
42. Rosenberg, M. F., Callaghan, R., Modok, S., Higgins, C. F., and Ford, R. C. (2005) Three-dimensional structure of P-glycoprotein, *J. Biol. Chem. 280*, 2857−2862.
43. Shilling, R., Federici, L., Walas, F., Venter, H., Velamakanni, S., Woebking, B., Balakrishnan, L., Luisi, B., and van Veen, H. W. (2005) A critical role of a carboxylate in proton conduction by the ATP-binding cassette multidrug transporter LmrA, *FASEB J. 19*, 1698.
44. Keniry, M. A., Gutowsky, H. S., and Oldfield, E. (1984) Surface dynamics of the integral membrane-protein bacteriorhodopsin, *Nature 307*, 383−386.
45. Herzfeld, J., Mulliken, C. M., Siminovitch, D. J., and Griffin, R. G. (1987) Contrasting molecular-dynamics in red and purple membrane-fractions of the *Halobacterium halobium*, *Biophys. J. 52*, 855−858.
46. Rothnie, A., Storm, J., Campbell, J., Linton, K. J., and Kerr, I. D. (2004) The topography of transmembrane segment six is altered during the catalytic cycle of P-glycoprotein, *J. Biol. Chem. 279*, 34913−34921.
47. Dong, J., Yang, G., and Mchaourab, H. S. (2005) Structural basis of energy transduction in the transport cycle of MsbA, *Science 308*, 1023−1028.
48. Lu, G., Westbrooks, J. M., Davidson, A. L., and Chen, J. (2005) ATP hydrolysis is required to reset the ATP-binding cassette dimer into the resting-state conformation, *Proc. Natl. Acad. Sci. U.S.A. 102*, 17969−17974.
49. Oswald, C., Holland, I. B., and Schmitt, L. (2006) The motor domains of ABC-transporters: What can structures tell us? *Naunyn-Schmiedebergs Arch. Pharmacol. 372*, 385−399.
50. Reyes, C. L., and Chang, G. (2005) Structure of the ABC transporter MsbA in complex with ADP-vanadate and lipopolysaccharide, *Science 308*, 1028−1031.
51. Wang, C., Karpowich, N., Hunt, J. F., Rance, M., and Palmer, A. G. (2004) Dynamics of ATP-binding cassette contribute to allosteric control, nucleotide binding and energy transduction in ABC transporters, *J. Mol. Biol. 342*, 525−537.
52. Higgins, C. F., and Linton, K. J. (2004) The ATP switch model for ABC transporters, *Nat. Struct. Mol. Biol. 11*, 918−926.

BI062109A